Optical and Quantum Electronics (2024) 56:771
https://doi.org/10.1007/s11082-024-06665-4

Investigation of SPR sensor for immunoglobulin detection by using Ag–Si_3N_4-BP on the sensing layer

Lokendra Singh[1] · Prakash Pareek[2] · Roshan Kumar[3] · Vipul Agarwal[5] · Naveen Kumar Maurya[2] · Amit Bage[4]

Received: 9 December 2023 / Accepted: 12 February 2024 / Published online: 25 March 2024

Abstract
Surface plasmon resonance (SPR) has gained attention as a promising method for effective label-free biosensing. Immunoglobulin (IgG) detection is very important to understand the past infection and immunity of any individual. Thus, this study aims to develop a SPR sensor with better sensitivity for detecting IgG. It emphasizes the utilization of a high-performance planar waveguide-based SPR sensor to detect IgG by analyzing a suitable sensor topology. The sensor configuration consists of five distinct layers: silver (Ag), silicon nitride (Si_3N_4), black phosphorus (BP), an enzyme, and a sensing medium. Silver (Ag) stimulates surface plasmons, while Si_3N_4 and BP are utilized to enhance absorption capabilities and serve as the bio-molecular recognition element, respectively. The proposed sensor simulation employs the transfer matrix method and an angular interrogation scheme. To assess this proposed sensor's impact, the sensing region is assessed while considering three layers: Ag, Ag-BP, and Ag–Si_3N_4. Initially, the thickness of the Ag layer is optimized by recording its transmittance and achieving a minimum transmittance of 0.0027 at a thickness of 50 nm. Subsequently, the performance parameters are assessed using four different structures with slight variations in the IgG samples. The results depict the maximum achieved sensitivities as follows: 192 °/RIU for conventional SPR, 203 °/RIU for BP-based SPR, 287 °/RIU for Si_3N_4-based SPR, and 352 °/RIU for the proposed structure. This comparative study demonstrates that the proposed SPR configuration significantly enhances sensitivity, quality factor, and detection accuracy performance.

Keywords Surface plasmon resonance · Immunoglobulin · Black phosphorus · Label free · Silicon nitride · Sensitivity · Transfer matrix method

1 Introduction

White blood cells include Immunoglobulin (IgG) glycoprotein molecules generated by plasma cells and offer infection protection. It can quickly identify viruses or bacteria. X-linked agammaglobulinemia and common variable immunodeficiency syndrome are two autoimmune and immunodeficiency illnesses for which IgG testing is crucial for the diagnosis. Therefore, the detection of IgG is a crucial regime of biosensing. In recent times,

Extended author information available on the last page of the article

IgG has been detected in the work by using a variety of techniques, including surface plasmon resonance (SPR), electrophoresis, radial immunodiffusion, and immunoblotting (Wu et al. 2016). A technologically advanced analytical instrument, the biosensor is capable of detecting minute biomolecules at low concentrations. For instance, the photonic crystal structure has been utilized in various ways to demonstrate biosensing applications (Yang et al. 2023; Najafgholinezhad and Olyaee 2014; Olyaee and Bahabady 2015; Bahabady and Olyaee 2015; Parandin et al. 2021; Gowdhami et al. 2022). However, detecting extremely low amounts of antibodies like IgG is a challenge for biosensors (Wu et al. 2016). Fortunately, the label-free nature of SPR biosensors makes them a promising tool. Furthermore, it offers the benefits of swift and precise detection, along with reliability. (Ravindran et al. 2023; Uniyal et al. 2023; Mudgal et al. 2023). SPR biosensors are now studied and investigated by using various structures and configurations (Bahri et al. 2022; Ebadi et al. 2020; Ben Salah et al. 2022a, b; Mao et al. 2017). Hence, it is vital to understand the basic classification of these sensors. Based on the coupling, these sensors are categorized into four types such as prism, optical fiber, waveguide, and grating-based.

Nowadays, the planar waveguide-based SPR sensor has also become popular in the detection of bio-molecular interactions like Deoxyribonucleic acid (DNA) and IgG (Mondal et al. 2023). SPR theory demonstrates that the optical light incident on the waveguide-metal interface at an angle greater than the critical angle. The light metal interaction leads to the generation of surface plasmons polaritons (SPPs). Further, the SPP oscillations set a surface plasmon wave (SPW) at the interface by applying the attenuated total reflection (ATR) (Homola et al. 1999). The SPW excites the evanescent waves, which exponentially decay in the orthogonal direction of the interface (Lee et al. 2007). These decaying waves are used for sensing the presence of bio-molecules at the sensor surface. However, prism-based sensor configurations were also utilized for similar applications due to simplicity, immunity to noise, and high sensitivity (Janith et al. 2023; Kushwaha et al. 2018a; Mudgal et al. 2020a).

On the other hand, distributed coupling can be used in a metal-coated waveguide as it offers better design flexibility and monolithic integration capabilities with existing SPR technology (Lavers et al. 2020; Kim et al. 2018). The ability to build compact, monolithic, and multi-sensor systems is specially provided by a planar waveguide (PWG) and is connected to instruments by using optical fibers. Additionally, these biosensors can be miniaturized to detect chemicals or biological agents in inaccessible places (Mukundan et al. 2009). PWG-based sensors feature a unique platform that enables the detection of a wide variety of samples in conjunction with imaging systems (Moznuzzaman et al. 2021; Cherouana et al. 2023). Moreover, they possess the potential for integration with optoelectronic components and the capacity to adjust the penetration depth of the evanescent field by varying the reflection angle. (Agnarsson et al. 2010). The inclusion of PWG with the SPR phenomenon leads to resonance oscillations of SPWs (Kashyap and Nemova 2009). As a result, minimal transmittance (T_{min}) occurs, which changes with the refractive index (RI) of the sensor surface and can be calculated using ATR (Pal et al. 2018). In general, to develop an SPR structure, a metal film comprising gold (Au) and silver (Ag) is typically deposited over the waveguide to facilitate Surface Plasmon (SP) propagation. Due to its high SPR ratio ($|\varepsilon_r/\varepsilon_i|$), Ag offers superior SPR performance, where ε_r and ε_i are the real and imaginary parts of the dielectric constant respectively (Sheng et al. 2019; Amirjani and Haghshenas 2018). In comparison to Au, Ag exhibits a steeper angular resonance curve, which indicates greater detection precision (Mitsushio et al. 2006; Beck et al. 2023). However, Ag lacks chemical stability, as evidenced by its quick oxidation (Jha and Sharma 2009). The inclusion of bimetallic, oxide, dielectric, and self-assembled monolayers can

prevent Ag from oxidation and sulfurization (Han et al. 2020). Preservation of Ag surfaces can be achieved through a self-assembled monolayer (SAM), which also enhances sample adherence to metal surfaces (Gahlaut et al. 2022). Dielectric materials can improve SPR performance, but it is difficult to preserve their intricate shape and optical characteristics. Some researchers have developed a hybrid structure with bimolecular recognizing elements (BREs) that offer excellent SPR performance (Yun et al. 2022; Hanson and Whelan 2023). In this work, a structure based on silicon nitride (Si_3N_4) has been presented to enhance the sensing capability of the sensor. The Si_3N_4 layer on top of the silver layer, provides immunity against oxidation. Moreover, the high refractive index of Si_3N_4 imparts excellent chemical, thermal, and biocompatibility qualities (Wu et al. 2016; Mudgal et al. 2022). To further enhance the sensing capability, two-dimensional (2D) materials like black phosphorus (BP) have been placed over the dielectric material, where they can act as a bio-molecular carrier as well as a protective layer. The unique mechanical and optoelectrical properties of BP, like higher bandgap, made it one of the most popular 2D materials in photonic sensors. In addition, BP boosts detection capabilities by enhancing interlayer coupling within the Van der Waals force. The higher absorption energy of BP makes it one of the potential candidates to be used for biomolecule binding (Nangare and Patil 2023).

In 2018, Kushwaha et al. introduced an SPR sensor for IgG detection that incorporated zinc oxide, gold, MoS_2, and Graphene, achieving a sensitivity of 101.5 °/RIU (Kushwaha et al. 2018b). Following this, in 2020, Mudgal et al. enhanced the sensitivity of the SPR sensor using zinc oxide, bimetallic materials, $BiTiO_2$, and graphene, reaching a sensitivity of 116.6 °/RIU (Mudgal et al. 2020a). Raikwar et al. in 2018 explored sensors based on gold and graphene oxide, attaining a sensitivity (S) of 143 °/RIU, a detection accuracy (DA) of 0.16, and a quality factor (QF) of 23.72 RIU^{-1} (Raikwar et al. 2020). Furthermore, Singh et al. in 2020 reported improved sensor performance by incorporating gold, blue phosphorus, MoS_2, and antimonide, achieving an S of 198 °/RIU and a DA of 0.15 (Singh et al. 2020).

Despite the various techniques and methods proposed for IgG detection, a strong demand remains for high-performance sensor technology in this field. This paper introduces an investigation of an SPR structure consisting of Ag, Si_3N_4, and BP to detect IgG using the transfer matrix method at a wavelength of 633 nm. The Ag layer is used due to its higher SPR ratio and provides better sensitivity as a substrate layer (Mudgal et al. 2020b). However, in the presence of biomolecules Ag gets oxidized, and hence reduces the lifetime of SPR biosensors (Qu et al. 2020). To overcome the oxidation issue, an anti-reflecting layer of Si_3N_4 is placed over it. Si_3N_4 got the attention because of its excellent chemical and thermal stability with a band gap of ~ 5 eV (Blázquez et al. 2014). Finally, a layer of BP is considered because of its ability to improve the adsorption rates, which is due to higher carrier mobility, interesting optical and electrical properties, and direct band gap (Blázquez et al. 2014).

The above brief survey of the literature reveals that dielectric materials, while capable of enhancing SPR performance, face challenges in maintaining their intricate shape and optical characteristics. Researchers have introduced a hybrid structure incorporating BREs for superior SPR performance. This work attempts to bring depth and novelty to the investigation of BRE-based structures by proposing a multilayer structure for the detection of IgG. Literature has not widely explored the effect of different configurations of hybrid structures. To evaluate the influence of the suggested sensor, an analysis of the sensing area is conducted, taking into account three layers: Ag, Ag-BP, and Ag–Si_3N_4. Each layer has a predefined role in the functioning of this biosensor. For instance, Si_3N_4 is utilized to boost sensing capability. To further elevate sensing capabilities, two-dimensional (2D) materials

like black phosphorus (BP) have been applied over the dielectric material, serving as a biomolecular carrier and protective layer.

The remainder of this article is structured into several sections as follows. Section 2 sheds light on various aspects of design considerations, including transmitting power, reflectivity, and performance parameters. Section 3 begins by presenting the scheme for optimizing the thickness of the sensing layer, followed by an analysis of the sensor's performance. The final subsection in this section highlights a comparison of this work with similar studies that have been reported. Finally, the last section, Sect. 4, concludes this work by emphasizing the significant findings of this study and discussing its potential future prospects.

2 Design considerations

This section explicates the proposed planar waveguide-based SPR sensor's design and analysis process, including mathematical equations and design parameters.

2.1 Transmitting power

Figure 1 shows the schematic of the considered PWG-based SPR sensor for IgG detection. The overall structure is divided into two sections: initially, a lossless single-mode single-layer waveguide is employed as the initial component to couple the incident light and generate surface plasmons (SPs). This segment is positioned at the exposed portion of the waveguide. In the second segment, the structure interacts with the test samples. The primary design constraints for a PWG-based SPR sensor include the appropriate substrate material and operating wavelength. The phase matching between waveguide and SP modes is attained due to the low-index glass substrate when the sensor operates in a liquid RI medium. To facilitate the fabrication of waveguides and to cut down the cost of raw slides, the substrate glass having an RI of 1.46 can be used (Rahman et al. 2017). Conversely, the investigation of a PWG SPR sensor is prompted by the stability and inertness of the metal layer to the external environment (Duveneck et al. 1997). However, the sensor's performance diminishes when there are changes in the optical properties of the metal film.

To create this biosensor (Raikwar et al. 2020), a dielectric slab was introduced between two layers with lower refractive indices. Both instances utilized the well-known optical phenomenon called Total Internal Reflection (TIR) to propagate and guide light along the

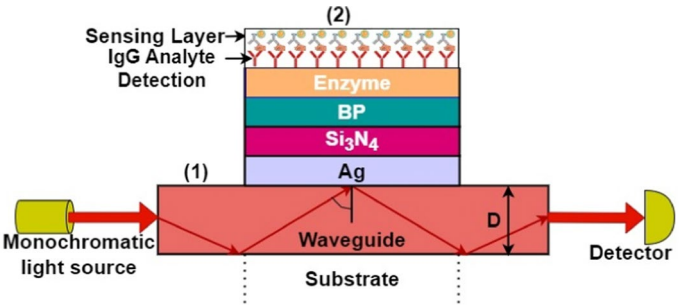

Fig. 1 Schematic of the proposed PWG-based SPR sensor

core. In this proposed setup, the first layer consisted of a waveguide with Ag immobilization, having a diameter represented as 'D.' Additionally, the third layer was composed of Si_3N_4, while the fourth and fifth layers were formed by BP and ELISA:oPD enzymes, respectively. The respective thicknesses of the layers of Ag, Si_3N_4, BP, and enzyme were denoted as d_2, d_3, d_4, and d_5. A light source was employed to emit a light beam with a central wavelength of 633 nm, which triggered surface plasmon polaritons (SPP) at the interface between the waveguide and the metal. The collected light was then directed to a spectrometer on the opposite side for analysis. Considering that a beam of power, P is launched at an angle of θ, and at the spectrometer, a power of dP is collected at an angle of dθ. Then, the mathematical expression for dP can be written as (Loan et al. 2014; Diéguez et al. 2009);

$$dP \propto P(\theta)d\theta \tag{1}$$

where P(θ) is the modal power proportional to the incident angle which is mathematically manifested in Eq. (2) (Hossain et al. 2021).

$$d\theta = \frac{n_c^2 \sin\theta\cos\theta}{\left(1 - n_c^2\cos^2\theta\right)^2} \tag{2}$$

where n_c is the RI of the core waveguide.

Furthermore, by using the reflectance value of the waveguide and metal interface, the normalized transmitted power for a single reflection can be written as (Hossain et al. 2021)

$$P_{trans} = \frac{\int_{\theta_{cr}}^{\pi/2} R_p^{N_{ref}(\theta)} P(\theta)d\theta}{\int_{\theta_{cr}}^{\pi/2} P(\theta)\, d\theta} \tag{3}$$

where $N_{ref}(\theta) = \frac{L}{D}\tan\theta$ is the summation of light reflections in the device, θ is the incident angle with the normal to the core metal layer interface in the sensing region of length L, and D is the diameter of the waveguide (Hossain et al. 2021). The transmitting power responses are plotted for the proposed structure by exploiting the angular interrogation technique to assess the sensor's performance. To investigate the structure RI of the designed parameters taken into consideration, such as Ag of 0.056206 + 4.2776i (Beck et al. 2023), Si_3N_4 of 2.0394 (Wu et al. 2016; Gahlaut et al. 2022), BP of (3.5 + 0.1iHossain et al. 2021), and an enzyme of 1.8 + 0.3i (Wu et al. 2016). The thickness of the metallic layer is optimized by following the iteration approach, whereas the thicknesses of Si_3N_4, BP, and enzyme layers are 5 nm, 0.53 nm, and 0.11 nm, respectively (Mudgal et al. 2022; Nangare and Patil 2023). Finally, the topmost layer of the sensor comprises the sensing medium in the presence of IgG with RI of 1.343 and 1.353 (Wu et al. 2016).

2.2 Reflectivity

Since the transfer matrix method (TMM) is an effective method that doesn't require any estimates, it is used to measure the reflectivity (R_p) of an N-layered structure. Here, the thickness and dielectric constant of the k^{th} layer along the z-axis are represented by d_k and ε_k, respectively. Additionally, the tangential fields derived by linking the boundary conditions (perfectly matched layers i.e. PML are used as boundary conditions with a meshing of

0.029 μm in both directions) demonstrate the relationship between the initial ($Z = Z_1 = 0$) and final ($Z = Z_{N-1}$) conditions as given in Eq. (4) (Nangare and Patil 2023):

$$\begin{bmatrix} P_1 \\ Q_1 \end{bmatrix} = H \begin{bmatrix} P_{N-1} \\ Q_{N-1} \end{bmatrix} \tag{4}$$

where, P_{N-1}, Q_{N-1}, $P_{1,}$ and Q_1 signify the N^{th} boundary tangential electrical and magnetic (EM) fields and the fields at the first layer boundary, respectively. The expression for the characteristics matrix (H_{ij}) of the proposed structure in the presence of a monochromatic light source with TM polarization is discussed in Eq. (5) (Yun et al. 2022). Furthermore, the transverse RI (l_k) and arbitrary stage constant (β_k) for the k^{th} layer are given by Eq. (6) and (7), respectively. The evaluation of wave impedance (Z_k) and input angle (θ_k) can be done by using Eq. (8) and (9), respectively.

$$H_{ij} = \left[\prod_{K=}^{N-1} \begin{pmatrix} \cos\beta_k & -i\varepsilon_k \sin\beta_k/\varepsilon_k \\ -i\varepsilon_k \sin\beta_k & \cos\beta_k \end{pmatrix} \right] = \begin{bmatrix} H_{11} & H_{12} \\ H_{21} & H_{22} \end{bmatrix} \tag{5}$$

where

$$l_k = \left[\frac{\mu_k}{\varepsilon_k} \right]^{1/2} \cos\theta_k = \sqrt{\frac{\varepsilon_k - \left(n_c \sin\theta\right)^2}{\varepsilon_k^2}} \tag{6}$$

and

$$\beta_k = \frac{2\pi}{\lambda} l_k \cos\theta_k \left(Z_k - Z_{k-1}\right) = \frac{2\pi}{\lambda} d_k \sqrt{\varepsilon_k - \left(n_c \sin\theta\right)^2} \tag{7}$$

$$Z_k = \frac{k_x l_k \cos\theta_k}{\left(2\pi c/\lambda_{633}\right)\varepsilon_k^2} \tag{8}$$

$$\theta_k = \left(\cos\sqrt{1 - \left(l_{k-1}/l_k\right)(\sin\theta)^2} \right)^{-1} \tag{9}$$

Parameters λ, μ_k, $\overrightarrow{k_x}$ and θ represent the wavelength, permeability, incident wave vector, and incident angle, respectively. The expression for calculating the reflection coefficient (r_p) and the Fresnel's mode (R_p) is described in Eq. (10) and (11), respectively:

$$r_p = \frac{\left(H_{11} + H_{12} l_n\right) - \left(H_{21} + H_{22} l_n\right)}{\left(H_{11} + H_{12} l_n\right) + \left(H_{21} + H_{22} l_n\right)} \tag{10}$$

$$R_p = \left| r_p \right|^2 \tag{11}$$

Here it is pertinent to note that the third-dimensional thickness of the suggested structure is considerably greater than the feature size within the computational plane (2D). Consequently, the impact of substrate thickness on the obtained outcomes can be disregarded by assuming, through mathematical means, that the structure is infinite in the third dimension (Ben Salah et al. 2019; Chao et al. 2021). As a result, all our

simulations are conducted in 2D, allowing for a substantial reduction in computational time without sacrificing calculation accuracy.

2.3 Performance parameters

In general, the performance of the SPR sensor is analyzed in terms of Sensitivity (S), Quality Factor (QF), and Detection Accuracy (DA). Parameter S is the ratio of change in resonance angle ($\nabla\theta_{res}$) to the RI (∇_n). The width of the SPR spectrum in context to 50% of maximum transmittance is known as Full Width at Half Maximum (FWHM). The ratio of sensitivity to FWHM describes QF. The ratio of $\nabla\theta_{res}$ and FWHM gives the value of DA. In addition, we have also evaluated the dip-figure of merit (DFOM), which is the ratio of S and minimum transmittance (T_{min}). The mathematical formulation of the parameters as mentioned earlier is given in Eqs. (12–15) (Han et al. 2020).

$$\text{Sensitivity (S)} \frac{\text{Change in resonance angle } \left(\nabla\theta_{res}\right)}{\text{Change in refractive index } (\nabla n)}{}^{\circ}/\text{RIU} \tag{12}$$

$$\text{QF} = \frac{\text{S}}{\text{Full width half maximum (FWHM)}} \left(\text{RIU}^{-1}\right) \tag{13}$$

$$\text{DA} = \frac{\nabla\theta_{res}}{\text{FWHM}} \tag{14}$$

$$\text{DFOM} = \frac{\text{S}}{\text{T}_{min}} \tag{15}$$

3 Results

3.1 Optimization of Ag thickness

To achieve the best performance of the structure, it's necessary to optimize the thickness of the Ag (silver) film. This optimization aims to maximize the absorption of energy from the optical signal, which is indicated by achieving minimum transmittance (T_{min}) performance (Sheng et al. 2019). Figure 2 depicts the transmittance responses for various Ag film thicknesses, ranging from 40 to 60 nm in 5 nm increments. Table 1 contains the estimated values of T_{min} and resonance angle (θ_{res}) for the data in Fig. 2. Notably, the lowest T_{min} value of 0.0027 and a θ_{res} of 81.10° are achieved when the Ag film thickness is 50 nm. As the thickness of the Ag film changes, θ_{res} shifts right, indicating that the proposed sensor exhibits Surface Plasmon Resonance (SPR) properties (Amirjani and Haghshenas 2018). Consequently, an Ag film thickness of 50 nm has been selected for further analysis of the proposed sensor.

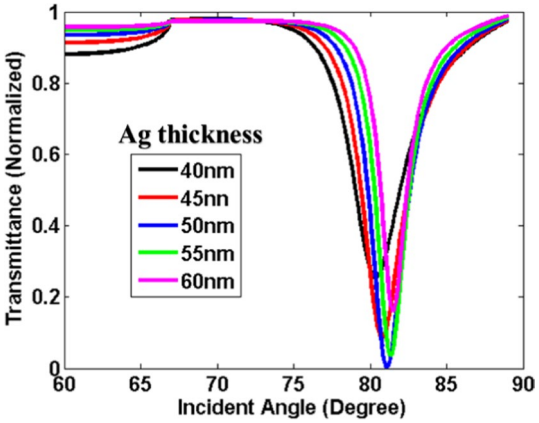

Fig. 2 Transmittance responses for the proposed sensor at different Ag thicknesses

Table 1 Transmittance and resolution angle versus Ag thicknesses

Ag thickness	T_{min}	θ_{res} (°)
40 nm	0.2546	80.35
45 nm	0.0850	80.80
50 nm	0.0027	81.10
55 nm	0.0349	81.34
60 nm	0.1605	81.48

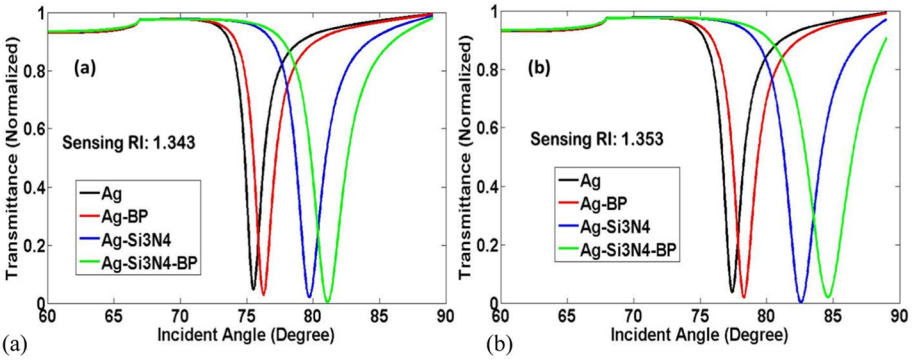

Fig. 3 Transmittance responses for all considered structures at sensing RI: **a** 1.343 and **b** 1.353

3.2 Sensing performance analysis

The impact of the proposed structure is assessed by comparing its performance to that of three other structures: Ag, Ag-BP, and Ag–Si_3N_4. In Fig. 3a and b, the transmittance responses of all these structures are displayed under sensing medium refractive indices (RIs) of 1.343 and 1.353, respectively. As the number of layers increases, the spectral width widens due to a damping effect. Specifically, the Full Width at Half Maximum (FWHM) values are 1.46, 1.68, 2.25, and 2.70 degrees for Ag, Ag-BP, Ag–Si_3N_4, and the

Table 2 Assessed parameters of θ_{res}, $\nabla\theta_{res}$ and ∇n for Fig. 3a and b

Structure	θ_{res} (°)		$\nabla\theta_{res}$ (°)	∇n
	$n_s = 1.343$	$n_s = 1.353$		
Ag	75.50	77.42	1.92	0.01
Ag-BP	76.26	78.29	2.03	0.01
Ag–Si_3N_4	79.71	82.58	2.87	0.01
Ag–Si_3N_4-BP	81.10	84.62	3.52	0.01

Table 3 Measured parameters of S, QF, DA and DFOM for Fig. 3a and b

Structure	Sensitivity (°/RIU)	QF (RIU^{-1})	DA	DFOM
Ag	192	131.51	1.31	4120.17
Ag-BP	203	120.83	1.21	7024.22
Ag–Si_3N_4	287	127.55	1.27	14422.11
Ag–Si_3N_4-BP	352	130.37	1.30	130370.37

proposed structure, respectively. The sensing of the analyte is carried out in two steps: in the first step, an RI of 1.343 is considered in the sensing medium, and transmittance curves for Ag, Ag-BP, Ag–Si_3N_4, and Ag–Si_3N_4-BP are plotted in Fig. 3a. For all the combinations the incident angle varied from 75.50 to 81.10°. Secondly, the transmittance curves are recorded for all the aforementioned structure combinations and the incident angle varies from 77.42 to 84.62°, and plotted in Fig. 3b.

The trend of T_{min} values is inversely proportional to the number of layers, resulting from variations in penetration lengths at the waveguide-metal interface. The obtained T_{min} values for Ag, Ag-BP, Ag-Si_3N_4, and the proposed structure are as follows: for Fig. 3a, they are 0.0466, 0.0289, 0.0199, and 0.0027, respectively. Similarly, in Fig. 3b, the T_{min} values are 0.0366, 0.0187, 0.0011, and 0.0203 for Ag, Ag-BP, Ag–Si_3N_4, and the proposed structure, respectively.

Resonance angles and their changes for Fig. 3 are detailed in Table 2. Furthermore, parameters related to SPR), such as Sensitivity (S), Quality Factor (QF), Detection Accuracy (DA), and Dip- Figure of Merit (DFOM), are evaluated using Eqs. (12–15) and are presented in Table 3. Notably, the proposed structure, Ag–Si_3N_4-BP, achieves the highest sensitivity of 352 °/RIU, surpassing conventional Ag, Ag-BP, and Ag–Si_3N_4 by 1.85, 1.73, and 1.23 times, respectively. This exceptional performance is attributed to the strong absorption capabilities of Si_3N_4 and BP (Homola et al. 1999; Mudgal et al. 2022). The proposed sensor configuration also provides wavelength flexibility, enhanced resolution, reduced cross-sensitivity, biocompatibility, longer lifetime, minimal signal damping, and improved integration. The layer of Si_3N_4 is also used to attain the anti-reflecting behavior that further resists the oxidation of Ag. Additionally, the performance improvement is due to the excellent optical properties and higher SPR ratio of Ag to confine SP to deep sub-wavelength and leading to sensitivity enhancement.

The QF and DA performances of the proposed structure are nearly on par with the conventional sensor due to the sharp resonance dip of Ag. They are approximately 1.07 and 1.02 times greater than the Ag-BP and Ag–Si_3N_4 structures, respectively. Moreover, the proposed structure boasts the highest DFOM, standing at 130,370.37. This value is significantly higher, being 31.64 times greater than the conventional structure, 18.56 times

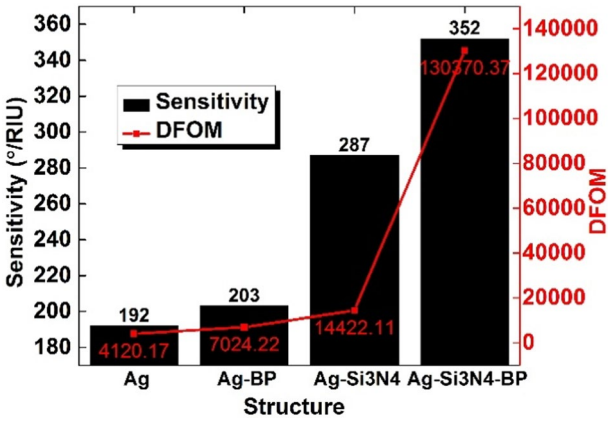

Fig. 4 Graphical representation of sensitivity and DFOM with respect to the structures

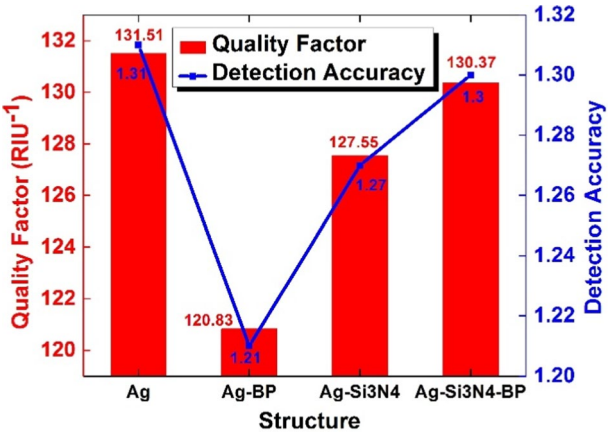

Fig. 5 Plots of QF and DA w.r.t the structures

greater than Ag-BP, and 9.04 times greater than Ag-Si_3N_4. For a visual representation of the SPR performance, including sensitivity and DFOM, please refer to Fig. 4. Additionally, Fig. 5 provides a graphical representation of the assessed QF and DA values for all structures. The QF and DA performances of the proposed structure are almost equal to the conventional sensor because of the sharp resonance dip of Ag. They are approximately 1.07 and 1.02 times greater than those of the Ag-BP and Ag-Si_3N_4 structures, respectively.

Similarly, the proposed structure has achieved the highest DFOM of 130370.37, which is 31.64, 18.56, and 9.04 times greater than the conventional, Ag-BP and Ag–Si_3N_4, respectively. The graphical representation of the computed SPR performance of sensitivity and DFOM for all structures is mentioned in Fig. 4. The representation of assessed QF and DA is provided in Fig. 5.

In addition, the selectivity test of the proposed sensor is also carried out in the presence of IgG, MCF cancer cells (n = 1.401), ring red blood cells (RBC) (n = 1.395), urea (n = 1.36) and DNA (n = 1.361). The selectivity test is done by recording the transmittance curve for all the used biomolecules as shown in Fig. 6. From the results, it can be observed that the transmittance for IgG molecules is nearly < 1% which is due to the presence of a specific enzyme. However, for other biomolecules, the transmittance is nearly > 30%.

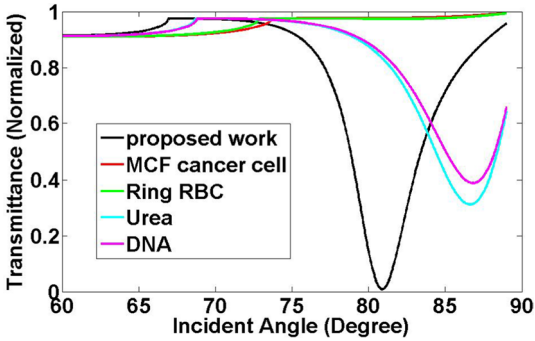

Fig. 6 Selectivity test of the proposed sensor

It may be relevant to mention here that in practical cases, plasmonic loses and fabrication imperfections play an important role in the sensor performance. In the context of planar waveguides, a crucial aspect is managing signal dispersion, particularly regarding the waveguide height, which is required to be above 200 nm. At greater heights, dispersion patterns align across frequencies, while at smaller heights, variations in dispersion curves become more pronounced (Syms and Solymar 2014). Achieving optimal waveguide thickness is essential for precise mode confinement. During fabrication, meticulous attention to layer deposition is necessary to prevent air bubbles and ensure a uniform distribution of metallic layers. Non-uniform distribution may lead to scattering, compromising the comprehensive confinement of optical signals and potentially reducing sensor performance.

3.3 Comparative study analysis

Finally, the performance of the proposed sensor is compared with recent existing sensors and reported in Table 4. This study reveals that the proposed sensor outperforms existing sensors in terms of Sensitivity (S), Quality Factor (QF), and Detection Accuracy (DA). The attained performance parameters are S of 352 °/RIU, QF of 130.37RIU^{-1} and DA of 1.30. Moreover, the proposed work has evaluated the performance of DFOM as a new SPR parameter and found that the maximum DFOM is 130370.37. Therefore, it can be concluded that the proposed PWG-based SPR sensor contributes a better SPR performance by utilizing the structure of Ag–Si_3N_4-BP to detect the bio-molecular interaction.

4 Conclusion

A high-performance planar waveguide-based SPR sensor for IgG detection has been presented in this work. The sensor structure consists of five layers: waveguide, Ag, BP, enzyme layer and sensing medium. To assess the impact of different design elements, three additional structures were investigated for performance analysis. The optimization process focused on the Ag thickness, leading to a minimum transmittance of 0.0027 achieved at an Ag thickness of 50 nm. Furthermore, the performance parameters were systematically analyzed across the four considered structures, considering minimal variations in IgG samples. Results show that the proposed structure, having Ag–Si_3N_4-BP as main constituents, has accomplished the highest sensitivity, 1.85, 1.73, and 1.23 times greater than the conventional Ag, Ag-BP and Ag–Si_3N_4, respectively. The comparative study with existing sensor

Table 4 Comparative study of the proposed and existing sensors

References	Structure	Sensitivity (°/RIU)	QF (RIU^{-1})	DA	DFOM
Kushwaha et al. (2018a)	Zinc Oxide–Au–MoS_2 –Graphene	101.5	–	–	–
Mudgal et al. (2020a)	Bimetallic–$BiTiO_2$ –Graphene	116.6	–	–	–
Raikwar et al. (2020)	Au–Graphene Oxide	143	23.71	0.16	–
Singh et al. (2020)	Au-blueP-MoS_2-Antimonene	194.8	–	0.15	–
Karki et al. (2022)	Prism-Ag-MXene-ZnO–Graphene	136.50	38.7	–	–
Islam et al. (2022)	Prism-Cr–Ag-BP-Graphene Oxide	352	76.48	–	–
Muthumanicam et al. (2023)	TiO_2–Cu–$BaTiO_3$	552	136.97	0.27	–
Rumi et al. (2024)	Al/BTO/Al/MoS_2	262	–	1.64	
Akib et al. (2024)	CaF_2–Cu–BP-Graphene	410	94.25	0.47	91.87
This work	Ag–Si_3N_4-BP	352	130.37	1.30	130370.37

structures is also explored, and it is observed that the proposed SPR amplifies the sensitivity and heightens the DFOM performance. Therefore, these findings suggest that the proposed SPR sensor, with its superior sensitivity and DFOM, holds great promise for IgG detection in the biomedical field. Notably this work can also be extended in future to investigate surface Immunoglobulin (SI_g) densities.

Author contributions LS conceptualized the whole idea and wrote the main manuscript, PP wrote the main manuscript and assisted LS; RK and VA prepared figures and abstract; NKM and AB prepared a literature review along with references.

Funding Not applicable.

Data availability Not Applicable.

Declarations

Conflict of interest The authors declare that they have no conflict of interests.

Ethical approval Not applicable.

References

Agnarsson, B., Halldorsson, J., Arnfinnsdottir, N., Ingthorsson, S., Gudjonsson, T., Leosson, K.: Fabrication of planar polymer waveguides for evanescent-wave sensing in aqueous environments. Microelectron. Eng. **87**, 56–61 (2010). https://doi.org/10.1016/j.mee.2009.05.016

Akib, T.B.A., Rana, M.M., Mehedi, I.M.: Multi-layer SPR biosensor for in-situ amplified monitoring of the SARS-CoV-2 omicron (B.1.1.529) variant. Biosens. Bioelectron.: X **16**, 1–13 (2024). https://doi.org/10.1016/j.biosx.2023.100434

Amirjani, A., Haghshenas, D.F.: Ag nanostructures as the surface plasmon resonance (SPR)- based sensors: a mechanistic study with an emphasis on heavy metallic ions detection. Sens. Actuat. B-Chem. **273**, 1768–1779 (2018). https://doi.org/10.1016/j.snb.2018.07.089

Bahabady, A.M., Olyaee, S.: Two-curve-shaped biosensor for detecting glucose concentration and salinity of seawater based on photonic crystal nano-ring resonator. Sens. Lett. **13**(9), 774–777 (2015). https://doi.org/10.1166/sl.2015.3517

Bahri, H., Hocini, A., Bensalah, H., Mouetsi, S., Ingebrandt, S., Pachauri, V., Hamani, M.: A high-sensitivity biosensor based on a metal–insulator–metal diamond resonator and application for biochemical and environment detections. Optik **271**, 1–9 (2022). https://doi.org/10.1016/j.ijleo.2022.170083

Beck, F., Loessl, M., Baeumner, A.J.: Signaling strategies of silver nanoparticles in optical and electrochemical biosensors: considering their potential for the point-of-care. Microchim. Acta **190**, 1–19 (2023). https://doi.org/10.1007/s00604-023-05666-6

Ben Salah, H., Hocini, A., Temmar, M., Khedrouche, D.: Design and analysis of mid-infrared high sensitive metal-insulator-metal plasmonic sensor. Chin. J. Phys. **61**, 86–97 (2019). https://doi.org/10.1016/j.cjph.2019.07.006

Bensalah, H., Hocini, A., Bahri, H.: Design and analysis of a mid-infrared ultra-high sensitive sensor based on metal-insulator-metal structure and its application for temperature and detection of glucose. Prog. Electromagn. Res. **2022**(112), 81–91 (2022a). https://doi.org/10.2528/PIERM22032604

Salah, H.B., Bahri, H., Hocini, A., Zegaar, I., Ingebrandt, S., Pachauri, V.: Design of a plasmonic sensor based on a nanosized structure for biochemical application. J. Phys. Conf. Ser. **2240**, 1–5 (2022b). https://doi.org/10.1088/1742-6596/2240/1/012024

Blázquez, O., López-Vidrier, J., Hernández, S., Montserrat, J., Garrido, B.: Electro-optical properties of non-stoichiometric silicon nitride films for photovoltaic applications. Energy Procedia. **44**, 145–150 (2014). https://doi.org/10.1016/j.egypro.2013.12.021

Chao, C.T., Chau, Y.F., Chiang, H.P.: Multiple Fano resonance modes in an ultra-compact plasmonic waveguide-cavity system for sensing applications. Res. Phys. **27**, 1–10 (2021). https://doi.org/10.1016/j.rinp.2021.104527

Cherouana, A., Benaissa, S., Bencheikh, A., et al.: Optimization of waveguide parameters for minimization of the sensitivity temperature dependence for the SiO2:TiO2 planar waveguide optical sensor. Opt. Quant. Electron. **55**, 1–21 (2023). https://doi.org/10.1007/s11082-023-05360-0

Diéguez, L., Darwish, N., Mir, M., Martínez, E., Moreno, M., Samitier, J.: Effect of the refractive index of buffer solutions in evanescent optical biosensors. Sens. Lett. **7**, 851–855 (2009). https://doi.org/10.1166/sl.2009.1161

Duveneck, G.L., Pawlak, M., Neuschäfer, D., Bär, E., Budach, W., Pieles, U., Ehrat, M.: Novel bioaffinity sensors for trace analysis based on luminescence excitation by planar waveguides. Sens. Actuat. B-Chem. **38**, 88–95 (1997). https://doi.org/10.1016/S0925-4005(97)80176-1

Ebadi, S.M., Örtegren, J., Bayati, M.S., Ram, S.B.: A multipurpose and highly-compact plasmonic filter based on metal-insulator-metal waveguides. IEEE Photonics J. **12**(3), 1–9 (2020). https://doi.org/10.1109/JPHOT.2020.2974959

Gahlaut, S.K., Pathak, A., Gupta, B.D., Singh, J.P.: Portable fiber-optic SPR platform for the detection of NS1-antigen for dengue diagnosis. Biosens. Bioelectron. **196**, 1–8 (2022). https://doi.org/10.1016/j.bios.2021.113720

Gowdhami, D., Balaji, V.R., Murugan, M., et al.: Photonic crystal based biosensors: an overview. ISSS J. Micro. Smart Syst. **11**, 147–167 (2022). https://doi.org/10.1007/s41683-022-00092-x

Han, L., Ding, H., Landry, N.N., Hua, M., Huang, T.: Highly sensitive SPR sensor based on Ag-ITO-BlueP/TMDCs-graphene heterostructure. Plasmonics **15**, 1489–1498 (2020). https://doi.org/10.1007/s11468-020-01165-z

Hanson, E.K., Whelan, R.J.: Application of the nicoya openSPR to studies of biomolecular binding: a review of the literature from 2016 to 2022. Sensors **23**(10), 1–22 (2023). https://doi.org/10.3390/s23104831

Homola, J., Yee, S.S., Gauglitz, G.: Surface plasmon resonance sensors: review. Sens. Actuat. B-Chem. **54**, 3–15 (1999). https://doi.org/10.1016/S0925-4005(98)00321-9

Hossain, B., Kabir, A., Rahman, M., Roy, S., Abdulrazak, L.F., Hossain, S., Mondol, N., Rahman, M.H., Islam, K.Z., Pathan, M.I.: Hybrid structure based high performance SPR sensor: a numerical approach of structure optimization for DNA hybridization. Opt. Quant. Electron. **53**, 1–9 (2021). https://doi.org/10.1007/s11082-020-02650-9

Islam, M.A., et al.: Design and analysis of GO coated high sensitive tunable SPR sensor for OATR spectroscopic biosensing applications. IEEE Access **10**, 103496–103508 (2022). https://doi.org/10.1109/ACCESS.2022.3211099

Janith, G.I., Herath, H.S., Hendeniya, N., Attygalle, D., Amarasinghe, D.A.S., Logeeshan, V., Wickramasinghe, P.M.T.B., Wijayasinghe, Y.S.: Advances in surface plasmon resonance biosensors for medical diagnostics: an overview of recent developments and techniques. J. Pharm. Biomed. Anal. Open **2**, 1–12 (2023). https://doi.org/10.1016/j.jpbao.2023.100019

Jha, R., Sharma, A.K.: Chalcogenide glass prism based SPR sensor with Ag–Au bimetallic nanoparticle alloy in infrared wavelength region. J. Opt. A-Pure Appl. Opt. **11**, 1–7 (2009). https://doi.org/10.1088/1464-4258/11/4/045502

Karki, B., Jha, A., Pal, A., et al.: Sensitivity enhancement of refractive index-based surface plasmon resonance sensor for glucose detection. Opt. Quant. Electron. **54**, 1–13 (2022). https://doi.org/10.1007/s11082-022-04004-z

Kashyap, R., Nemova, G.: Surface plasmon resonance-based fiber and planar waveguide sensors. J. Sens. **2009**, 1–9 (2009). https://doi.org/10.1155/2009/645162

Kim, K.-J., Lu, P., Culp, J.T., Ohodnicki, P.R.: Metal-organic framework thin film coated optical fiber sensors: a novel waveguide-based chemical sensing platform. ACS Sensors **3**, 386–394 (2018). https://doi.org/10.1021/acssensors.7b00808

Kushwaha, A.S., Kumar, A., Kumar, R., Srivastava, M., Srivastava, S.: Zinc oxide, gold and graphene-based surface plasmon resonance (SPR) biosensor for detection of pseudomonas like bacteria: a comparative study. Optik **172**, 697–707 (2018a). https://doi.org/10.1016/j.ijleo.2018.07.066

Kushwaha, A., Hans, N., Kumar, S., Rani, R.: A critical review on speciation, mobilization and toxicity of lead in soil-microbe-plant system and bioremediation strategies. Ecotoxicol. Environ. Safe **147**, 1035–1045 (2018b). https://doi.org/10.1016/j.ecoenv.2017.09.049

Lavers, C.R., Itoh, K., Wu, S.C., Murabayashi, M., Mauchline, I., Stewart, G., Stout, T.: Planar optical waveguides for sensing applications. Sens. Actuat. B-Chem. **69**, 85–95 (2000). https://doi.org/10.1016/S0925-4005(00)00412-3

Lee, K.L., Lee, C.W., Wang, W.S., Wei, P.K.: Sensitive biosensor array using surface plasmon resonance on metallic nanoslits. J Biomed. Opt. **12**, 1–5 (2007). https://doi.org/10.1117/1.2772296

Loan, P.T.K., Zhang, W., Lin, C.T., Wei, K.H., Li, L.J., Chen, C.H.: Graphene/MoS2 heterostructures for ultrasensitive detection of DNA hybridization. Adv. Mater. **26**, 4838–4844 (2014). https://doi.org/10.1002/adma.201401084

Mao, J., Zhai, X., Wang, L., Li, H.: Numerical analysis of near-infrared plasmonic filter with high figure of merit based on Fano resonance. Appl. Phys. Express **10**(8), 1–11 (2017). https://doi.org/10.7567/APEX.10.082201

Mitsushio, M., Miyashita, K., Higo, M.: Sensor properties and surface characterization of the metal-deposited SPR optical fiber sensors with Au, Ag, Cu, and Al. Sens. Actuat. A-Phys. **125**, 296–303 (2006). https://doi.org/10.1016/j.sna.2005.08.019

Mondal, H.S., Ahmed, K.A., Birbilis, N., et al.: Machine learning for detecting DNA attachment on SPR biosensor. Sci. Rep. **13**, 1–10 (2023). https://doi.org/10.1038/s41598-023-29395-1

Moznuzzaman, M., Islam, M.R., Khan, I.: Effect of layer thickness variation on sensitivity: an SPR based sensor for formalin detection. Sens. Bio-Sens. Res. **32**, 1–10 (2021). https://doi.org/10.1016/j.sbsr.2021.100419

Mudgal, N., Yupapin, P., Ali, J., Singh, G.: BaTiO3-Graphene-affinity layer-based surface plasmon resonance (SPR) biosensor for pseudomonas bacterial detection. Plasmonics **15**, 1221–1229 (2020a). https://doi.org/10.1007/s11468-020-01146-2

Mudgal, N., Saharia, A., Choure, K.K., Agarwal, A., Singh, G.: Sensitivity enhancement with anti-reflection coating of silicon nitride (Si3N4) layer in silver-based surface plasmon resonance (SPR) sensor for sensing of DNA hybridization. Appl. Phys. A **126**, 1–8 (2020b). https://doi.org/10.1007/s00339-020-04126-9

Mudgal, N., Choure, K.K., Falaswal, M.K., et al.: Impact of Taguchi optimization in fiber surface plasmon resonance sensors based on Si3N4 layer. Braz. J. Phys. **52**, 1–10 (2022). https://doi.org/10.1007/s13538-022-01088-6

Mudgal, N., Sahara, A., Agarwal, A., Singh, G.: ZnO and Bi-metallic (Ag–Au) layers based surface plasmon resonance (SPR) biosensor with BaTiO3 and graphene for biosensing applications. IETE J. Res. **69**, 932–939 (2023). https://doi.org/10.1080/03772063.2020.1844074

Mukundan, H., Kubicek, J.Z., Holt, A., Shively, J.E., Martinez, J.S., Grace, K., Grace, W.K., Swanson, B.I.: Planar optical waveguide-based biosensor for the quantitative detection of tumor markers. Sens. Actuat., B Chem. **138**, 453–460 (2009). https://doi.org/10.1016/j.snb.2009.01.073

Muthumanicam, M., Vibisha, A., Lordwin Prabhakar, M.C., Suresh, P., Rajesh, K.B., Jaroszewicz, Z., Jha, R.: Numerical investigation on high-performance Cu-based surface plasmon resonance sensor for biosensing application. Sensors **23**(17), 1–15 (2023). https://doi.org/10.3390/s23177495

Najafgholinezhad, S., Olyaee, S.: A photonic crystal biosensor with temperature dependency investigation of micro-cavity resonator. Optik **125**, 6562–6565 (2014). https://doi.org/10.1016/j.ijleo.2014.08.043

Nangare, S., Patil, P.: Black phosphorus nanostructure based highly sensitive and selective surface plasmon resonance sensor for biological and chemical sensing: a review. Crit. Rev. Anal. Chem. **53**, 1–26 (2023). https://doi.org/10.1080/10408347.2021.1927669

Olyaee, S., Bahabady, A.M.: Design and optimization of diamond-shaped biosensor using photonic crystal nano-ring resonator. Optik **126**(20), 2560–2564 (2015). https://doi.org/10.1016/j.ijleo.2015.06.037

Pal, S., Verma, A., Raikwar, S., Prajapati, Y.K., Saini, J.P.: Detection of DNA hybridization using graphene-coated black phosphorus surface plasmon resonance sensor. Appl. Phys. A-Mater. **124**, 394 (2018). https://doi.org/10.1007/s00339-018-1804-1

Parandin, F., Heidari, F., Rahimi, Z., Olyaee, S.: Two-dimensional photonic crystal biosensors: a review. Opt. Laser Technol. **144**, 1–45 (2021). https://doi.org/10.1016/j.optlastec.2021.107397

Qu, G., Xia, T., Zhou, W., Zhang, X., Zhang, H., Hu, L., Shi, J., Yu, X.-F., Jiang, G.: Property–activity relationship of black phosphorus at the nano–bio interface: from molecules to organisms. Chem. Rev. **120**, 2288–2346 (2020). https://doi.org/10.1021/acs.chemrev.9b00445

Rahman, M.S., Anower, M.S., Hasan, M.R., Rikta, K.A.: Design and analysis of graphene coated planar waveguide based surface plasmon resonance biosensor. Sens. Lett. **15**, 485–491 (2017). https://doi.org/10.1166/sl.2017.3843

Raikwar, S., Prajapati, Y.K., Srivastava, D.K., Saini, J.P.: Graphene oxide based SPR sensor for sensing of sea water concentration. Res. Opt. **1**, 1–5 (2020). https://doi.org/10.1016/j.rio.2020.100011

Ravindran, N., Kumar, S., Yashini, M., Rajeshwari, S., Mamathi, C.A., Thirunavookarasu, S.N., Sunil, C.K.: Recent advances in surface plasmon resonance (SPR) biosensors for food analysis: a review. Crit. Rev. Food Sci. Nutr. **63**, 1055–1077 (2023). https://doi.org/10.1080/10408398.2021.1958745

Rumi, R.B., Paul, A.K., Alyami, S.A., Moni, M.A.: Multi-disease detection using a prism-based surface plasmon resonance sensor: a TMM and FEM approach. IEEE Trans. Nanobiosci. **23**, 51–62 (2024). https://doi.org/10.1109/TNB.2023.3286269

Sheng, X., Liu, J., Yang, H., Chen, L., Li, J., Liu, H.: Optimization of tunable symmetric SPR sensor based on Ag-graphene. Optik **184**, 339–347 (2019). https://doi.org/10.1016/j.ijleo.2019.04.076

Singh, M.K., Pal, S., Prajapati, Y.K., Saini, P.: Sensitivity improvement of surface plasmon resonance sensor on using BlueP/MoS2 heterostructure and antimonene. IEEE Sens. Lett. **4**, 1–4 (2020). https://doi.org/10.1016/j.rio.2020.100011

Syms, R.R.A., Solymar, L.: Loss and thermal noise in plasmonic waveguides. J. Appl. Phys. **115**, 1–12 (2014). https://doi.org/10.1063/1.4880663

Uniyal, A., Srivastava, G., Pal, A., et al.: Recent advances in optical biosensors for sensing applications: a review. Plasmonics **18**, 735–750 (2023). https://doi.org/10.1007/s11468-023-01803-2

Wu, Q., Song, D., Zhang, D., Sun, Y.: An enhanced SPR immunosensing platform for human IgG based on the use of silver nanocubes and carboxy-functionalized graphene oxide. Microchim. Acta **183**, 2177–2184 (2016). https://doi.org/10.1007/s00604-016-1853-0

Yang, Y., Xiang, Y., Qi, X.: Design of photonic crystal biosensors for cancer cell detection. Micromachines. 1–11 (2023). https://doi.org/10.3390/mi1407147

Yun, C., Shun, M., Jackson, K., Newiduom, L., Browndi, I.: The use of bilayers consisting of graphene and noble metals has been explored for biosensors that employ inverted surface plasmon resonance. Int J Sci Inf Syst **12**, 441–449 (2022)

Authors and Affiliations

Lokendra Singh[1] · Prakash Pareek[2] · Roshan Kumar[3] · Vipul Agarwal[5] · Naveen Kumar Maurya[2] · Amit Bage[4]

✉ Prakash Pareek
ppareek1@gmail.com

Lokendra Singh
kashyap00000@gmail.com

Roshan Kumar
roshan.iit123@gmail.com

Vipul Agarwal
agarvipul@gmail.com

Naveen Kumar Maurya
naveen.maurya222@gmail.com

Amit Bage
abage@nith.ac.in

[1] Department of Electronics and Communication Engineering, Graphic Era (Deemed to be University), Dehradun, Uttrakhand 248002, India

[2] Department of Electronics and Communication Engineering, Vishnu Institute of Technology, Bhimavaram, Andhra Pradesh 534202, India

[3] Henan University, Kaifeng, Henan 475001, China

[4] Department of Electronics and Communication Engineering, National Institute of Technology Hamirpur, Hamirpur, Himachal Pradesh 177005, India

[5] Department of Electronics and Communication Engineering, Koneru Lakshmaiah Education Foundation (KLEF), Vaddeswaram, Andhra Pradesh 522302, India